

STUDY OF THE HEATING OF A HYPERSONIC PROJECTILE THROUGH A MULTIDISCIPLINARY SIMULATION

J. Bartolomé Calvo*, A. Mack* and O. Bozic*

*DLR, German Aerospace Center
Lilienthalplatz 7, D-38108 Braunschweig, Germany
e-mail: Javier.BartolomeCalvo@dlr.de

Key words: Aerothermodynamics, Multidisciplinary simulation, Railgun, Hypersonic

Abstract. *This document presents the results of a coupled fluid-thermal simulation along the trajectory of an hypersonic projectile for different surface coatings. These kind of simulations will become necessary to reliably design the thicknesses of the Thermal Protection System (TPS) of hypersonic vehicles. The considered vehicle is a suborbital projectile launched by a Railgun. The projectile is non-propelled and reaches an altitude of 115 Km, where it leaves its payload. To reach the desired altitude, the projectile has to be accelerated at the Railgun reaching a Mach number of 6,2 at the outlet of the canyon. To determine the temperature evolution of the vehicle, the firsts instants of the trajectory have to be accurate simulated. Therefore, a coupled simulation, which provides a better estimation of the maximal temperature of the projectile is performed. The strategy to obtain the unsteady evolution of the temperature is done in different phases. At first a steady state coupled simulation is performed to see the behavior of the algorithm, followed by an unsteady simulation for the first point of the trajectory of the vehicle to see if the model reaches a steady state. Finally, unsteady simulations, which are then compared with a classical pre-design engineering method are described. The results show that the maximal temperature reached by the projectile is much lower than the radiative equilibrium at the beginning of the trajectory. The classical pre-design engineering method shows the same type of temperature profile but the maximal temperature is higher than in a coupled simulation due to the simplified model.*

1 INTRODUCTION

A body moving at hypersonic speed develops a front shock wave around its front part, as shown in Fig. 1a. The air is compressed, heated, and decelerated by this shock. At the nose region of the body, a large convective heat transfer occurs. Consequently, a heat flux develops from the hot air flow behind the shock to the body surface, which is conducted to its inner parts. The nose of the body can be extremely heated depending on many factors, such as the flight time, the surface material, and its geometry. A reliable and accurate design of the body structure needs the coupling of flow and structure codes to analyse the thermal behaviour of the vehicle. Indeed, a coupled analysis of the body heating is interesting to know the maximal temperature that the vehicle reaches, as well as its unsteady evolution. The main difference of a coupled simulation with respect to a Computational Fluid Dynamics (CFD) analysis is that in the first case the amount of heat which is conducted into the structure and along the surface is taken into account. For the purpose of the present study, multidisciplinary simulations are performed by means of a DLR software environment which couples flow and structure codes, developed within the IMENS (Integrated Multi-disciplinary dEsign of hot Structures) project, which is part of the German ASTRA program.

The work is based around the thermal behaviour of a hypersonic vehicle. A surface placed in a hypersonic flow has two types of energetic exchanges: convection and radiation. If the sum of the received and emitted fluxes at the surface is negative, the difference is dissipated in the form of conduction through the wall, or eventually by ablation of the material, not considered in this study. The general heat balance equation of a hypersonic vehicle is:

$$\dot{q}_{Conv} - \dot{q}_{Radiation-wall} + \dot{q}_{Rad-gas-wall} = \dot{q}_{Conduction} + \dot{q}_{Ablation} \quad (1)$$

where the subscripts: *Conv* is referred to the convective heat flux, *Radiation-wall* to the radiative heat flux from the surface of the vehicle to the gas, *Rad-gas-wall* to the radiation from the gas to the wall, *Conduction* to the conductive heat flux, and *Ablation* to the ablative heat flux. When the surface is at a steady state, the temperature of the wall tends to a value that equals the balance of convective and the radiative heat fluxes, the temperature is then called radiative equilibrium temperature. But when the flow conditions change, this balance is disturbed and the difference of heat fluxes is transmitted by conduction through the wall. That is the case in a trajectory of the vehicle. Furthermore, for the studied projectile, at the beginning of its trajectory the convective heat flux is transferred fast completely by conduction because the surface of the vehicle is at the ambient temperature. The analysis of the coupled simulation is divided in two parts in order to understand all the phenomena at which the hypersonic body is exposed. At first, a steady state analysis is performed. After obtaining the results of this analysis, a time dependent simulation to obtain the evolution of the temperature over the trajectory is performed and compared to a classical pre-design engineering method.

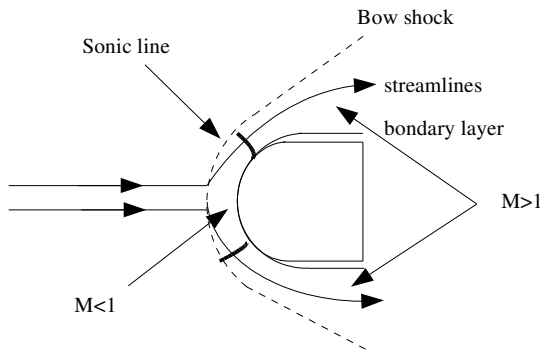


Figure 1: a) Hypersonic flow around a blunt body. b) Image of the suborbital Railgun projectile.

2 TRAJECTORY AND STRUCTURE DESCRIPTION

The projectile to be launched by a Railgun here considered, Fig. 1b, is completely described in reference 1. Other versions of this projectile that permit the placement of heavier payloads into orbit are described in reference 2. All the foreseen configurations, whether propelled or non-propelled, leave the gun at a hypersonic speed. The geometrical main differences are the diameter and the length of the projectiles. In all the cases the maximum thermal and mechanical loads happen in the first instants of the trajectory.

The studied projectile shall deploy meteorological payloads into suborbital altitudes, as the current miniaturized sounding rocket experiments. The trajectory and the design of the projectile² has been calculated to place a maximum payload mass of 400g within a volume of 270 cm³ at an altitude of 115 Km. In Fig. 2a the velocity and the altitude profiles during the trajectory of the vehicle are presented.

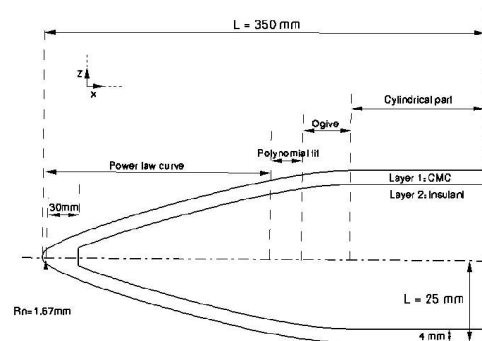
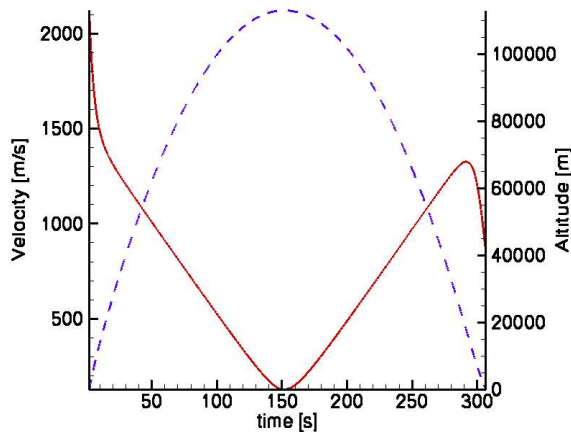


Figure 2: a) Description of the trajectory of the suborbital projectile, altitude and velocity versus time. b) Description of the structure and the geometry of the nosecap.

The most loaded parts of the projectile are the front part and the leading edges of the fins. The projectile is exposed to a severe environment at the firsts instants of the trajectory. Indeed, the heat flux at hypersonic speeds is proportional to the density and to the cube of the velocity. For this vehicle, both quantities are maximal at the beginning of the trajectory. For the purpose of studying the heating of the projectile, just the nosecone has been considered. The geometry is presented in Fig. 2b; the radius of curvature is $R_n = 1,67$ mm, followed by a power law curve optimised for Mach number 6,2, then a polynomial fitting curve which joins an ogival curve, and finally the cylindrical part. The foreseen nosecone structure is also shown in Fig. 2b; it has an initial bulk part of 30 mm, and the thickness of the ceramic material in the rest is 4 mm.

Two different Ceramic Matrix Composites (CMC) are considered for the outer layer: Carbon Reinforced Silicon Carbide³ (C/C-SiC), and Wound Highly Porous Oxide Composite⁴ (Whipox). For the interior part, in both cases an insulation material which has a very low thermal conductivity and low density has been considered. Both materials were chosen because of their different properties. The C/C-SiC presents a high thermal conductivity, which transports the heat to the inner parts of the structure, and it also presents an excellent emissivity coefficient. In comparison to this properties, the Whipox material presents a lower thermal conductivity, as well as a lower emissivity coefficient. Since the characteristics are quite different, the numerical simulations shall show the difference in the heating of the projectile depending on the material properties.

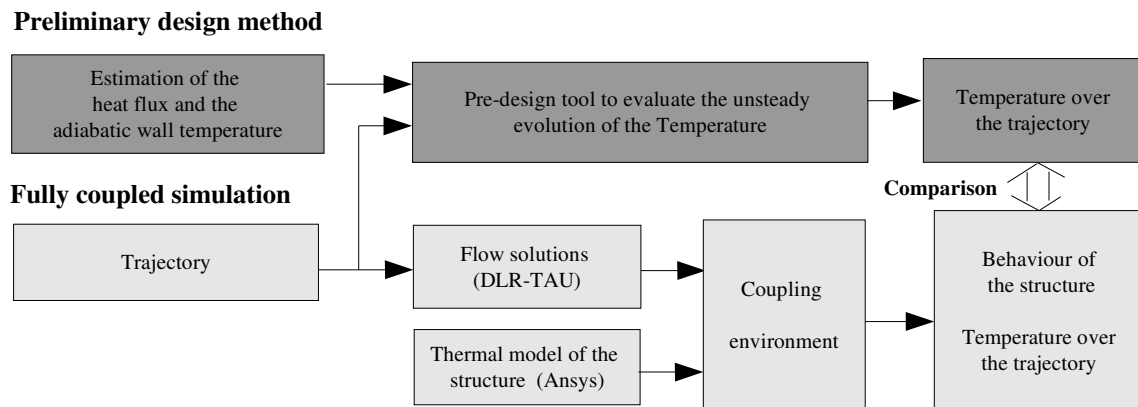


Figure 3: Description of the study.

The purpose of the work, summarised in Fig. 3, is to compare two different approaches which give the temperature at the stagnation point and inside the structure along the trajectory of the vehicle. The first approach is the classical pre-design engineering method which uses a Fay-Riddell expression in addition to analytical solutions of the heat diffusion equation. It estimates the temperature at the surface of the vehicle along the trajectory. The second and complete approach is a fully flow/thermal coupled simulation of the projectile along its

trajectory. As a preparation of this simulation, some flow solutions and a thermal model of the structure have to be developed and validated. Then, joining both computational models with the IMENS coupling tool, the evolution of the temperature along the trajectory is calculated. Finally and as a conclusion, the results of both methods are compared.

3 THE PRE-DESIGN METHOD

The pre-design engineering method is based on stagnation point predictions, like the FayRiddell method⁴ plus an analytical solution of the heat diffusion equation to update the value of the temperature at the surface. The time is discretised in intervals, and within each time interval the heat flux is considered to be constant, obtaining the temperature at the end of the time step. The convective heat flux, which is a function of the free-stream conditions, the properties and current temperature of the wall, is estimated and applied as a Boundary Condition (BC) to the analytical one-dimensional solution of the differential equation. Using the analytical solution, the temperatures associated to this heat flux in a time interval are estimated. This procedure is repeated along the trajectory of the vehicle estimating the temperatures at each time step. The heat diffusion equation is:

$$\frac{\partial T}{\partial t} = k \frac{\partial^2 T}{\partial x^2} \quad \text{with} \quad k = \frac{\lambda}{\rho C} \quad (2)$$

where k is the thermal diffusivity, λ the thermal conductivity, C the heat capacity, and ρ the density. Two models are used to calculate the evolution of the temperature, an infinite and a finite wall models. The first analytical solution⁵ corresponds to the infinite wall model, as it is seen in the BCs: heat flux BC at the surface of the wall, and no increment of temperature when x tends to infinity.

$$\frac{\partial T}{\partial t}(0, t > 0) = -\frac{\dot{q}(0, t)}{\lambda}, \quad \Delta T(x, t < 0) = \Delta T(\infty, t > 0) \quad (3)$$

These BCs lead to the following solution:

$$T(x, t) = T_0 + \frac{\dot{q}}{\sqrt{\rho c \lambda}} \left[2\sqrt{\frac{t}{\pi}} \exp\left(\frac{-x^2}{4kt}\right) - \frac{x}{\sqrt{k}} \operatorname{erfc}\left(\frac{x}{2\sqrt{kt}}\right) \right] \quad (4)$$

The finite wall model has also a heat flux BC at the surface of the wall (in this case $x=L$), but an adiabatic condition at the end of the wall ($x=0$):

$$\frac{\partial T}{\partial t}(x=L, t) = -\frac{\dot{q}}{\lambda}, \quad \frac{\partial T}{\partial t}(x=0, t) = 0 \quad (5)$$

This BCs lead to the following solution, which in the computational implementation is truncated:

$$T(x, t) = T_0 + \frac{\dot{q}L}{\lambda} \left[\frac{kt}{L^2} + \frac{1}{2} \left(\frac{x}{L} \right)^2 - \frac{1}{6} - 2 \sum_{n=1}^{\infty} \frac{(-1)^n}{(\delta_n L)^2} \exp(-\lambda \delta_n^2 t) \cos(\delta_n x) \right] \quad \delta_n = n \frac{\pi}{L} \quad (6)$$

4 COMPUTATIONAL METHODS AND ALGORITHM DESCRIPTION

To perform a coupled simulation, the flow solver DLR-Tau, the structural solver Ansys, in addition to the coupling tool developed within the IMENS project, which uses the commercial Multi-mesh Based Code Coupling Interface (MpCCI) interpolation routine have been used. A briefly description of the codes and tools is done here.

Flow solver DLR-Tau Code: it is an unstructured finite volume code developed completely at DLR to obtain an efficient and accurate solution of the Euler/Navier-Stokes equations for subsonic, transonic, and hypersonic flows⁷. In this study, all fluid solutions are performed using a perfect gas model for air. The catalicity of the wall has not been taken into account because the temperature behind the bow shock has a maximum value of 2500K. And at the pressure of 1 atm the O₂ begins to dissociate at a 2500K⁸. Therefore, there would be just few changes in the concentration of the oxygen in the boundary layer, but these effects would be less significant than in a reentry trajectory. Moreover, the small shock stand-off due to the small noscap radius causes the chemical degrees of freedom to be negligible. To reduce the computational time of the simulation approximately 4 times, an axially symmetrical model has been used. This has also the advantage, that the shock wave resolution, which has a length of some free mean paths, can be better performed.

Ansys: it is a commercial development and an analysis software which uses the Finite Element Theory. This software allows to study the physical behavior of a structure model to a set of initial and boundary conditions applied by the user. It allows different types of analysis: structural, thermal, and electromagnetic, although just the thermal analysis is used. In this case, also an axially symmetrical model has been used, conduction, as well as radiation to the free space are considered in the model. But the deformation of the structure due to the thermo-mechanical loads has not been taken into account.

Surface Interpolation Routine MpCCI: It is an interpolation routine developed by the Fraunhofer Institute, and designed to couple different simulation codes. In this case, it enables to couple the flow and the structural solvers. This interpolation routine has the advantage of taking the maximum profit of the discretisation domains used by the different codes, which have been optimised separately for its domains of application.

Coupling procedure: it is a loose coupled approach, in which the solutions are performed using different schemes, as shown in Fig. 4. In the present study, the CFD solver DLR-Tau calculates the surface heat flux, then its solution is interpolated using MpCCI and set as the BC of the structural solver Ansys. The structural solver gives the temperature associated with the applied heat flux, which is then interpolated and set as BC to the flow solver. The DLR-Tau computes the associated heat flux. This is called Dirichlet-Neumann iteration and is

applied with a relaxation of the temperature for the steady state case, and looped over time for the unsteady simulation over the trajectory. The only parameter which changes from the steady to the unsteady is the type of analysis made by the structural solver, in one case steady and in the other one unsteady within a time interval. This procedure is repeated iteratively until a convergence of the algorithm has been reached. Typically, an accurate solution is achieved within 3 to 5 iterations for steady and in 2 to 3 for the unsteady simulations depending on the time step and the variation of the temperature. This tool and the iterative procedure have already been tested and validated in the past for hypersonic flows^{9,10}.

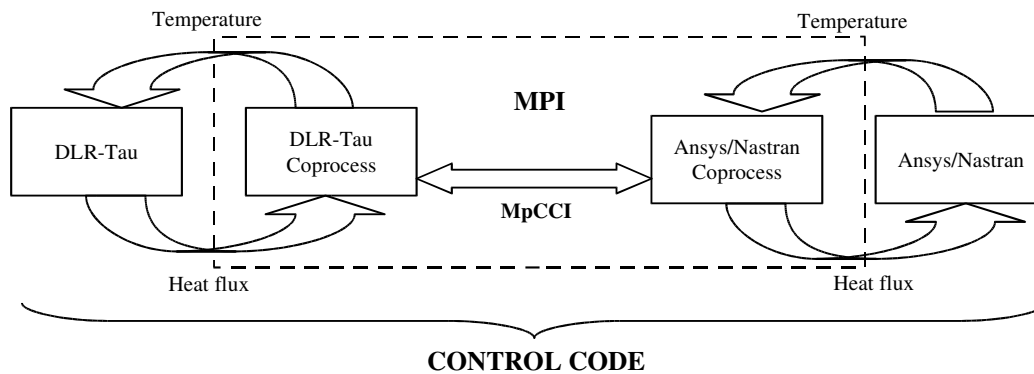


Figure 4: Coupling procedure⁹.

A loose coupling method, solving the fluid-dynamic steadily and the thermal behavior of the structure unsteadily will provide accurate results if the ratio between the characteristic times¹¹ of the thermal conduction and the fluid-dynamic is small. This ratio, where k is the thermal diffusivity of the material, V the velocity, and R_n the curvature radius of the wall, can be calculated using the following expression:

$$\frac{t_{fluid}}{t_{thermal}} = \frac{k}{R_n V} \quad (7)$$

For the selected materials, this ratio is in the order of 10^{-6} , meaning that fluid-dynamic characteristic is many times slower than the thermal one. Indeed, different flow solutions at different instants of the trajectory over the trajectory show that the temperature and the heat flux curves along the projectile are simply parallel, which shows that the flow topology around the nose of the projectile can be considered as steady.

For the simulation of the projectile along its trajectory, the domain of interest for the thermal loads is limited up to 40 Km since above these altitude the density of the air is very low. Hence, just the first 30 seconds of the trajectory have been calculated. Furthermore, up to this altitude, the temperature of the projectile will be moderately low, under 1000 K.

In order to calculate the unsteady evolution of the temperature, the algorithm described in Fig. 5 is implemented. The process starts computing a flow solution setting the temperature at

the surface and inside the projectile to the normal atmosphere temperature, approximately 300K. The heat flux is calculated at each time interval (t_{it} , $t_{it}+\Delta t_{it}$) setting as BC the temperature at the surface of the projectile. It is assumed that within the time interval the temperature is constant. The resulted heat flux is then applied as BC to the thermal solver, and a transient analysis is performed to calculate the temperature at the nose cap at $t_{it}+\Delta t_{it}$. While for the steady, case 1, the temperature at applied to the flow solver is quite relaxed to guarantee a smooth convergence, for the unsteady case, choosing properly the time steps, the relaxation factor may be set to a near value of 1.

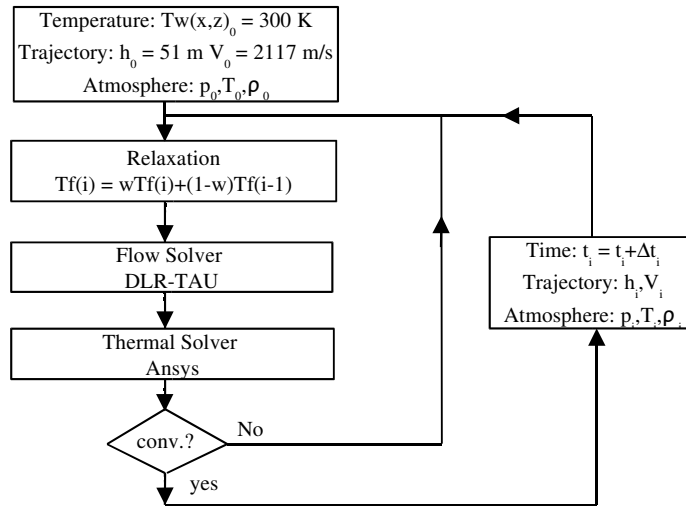


Figure 5: Algorithm to calculate the unsteady evolution of the temperature along the trajectory.

The convergence criteria in each time step is the following:

$$\epsilon = \frac{|T_f(i) - T_f(i-1)|^2}{|T_f(i-1)|^2} \quad (8)$$

where T_f is the fluid temperature. If the error is lower than a defined value, in this case 10^{-2} , the algorithm is considered to be converged. Then, according to the time step, the velocity and the altitude of the projectile, as well as the atmospheric characteristics are updated and a new iteration begins. The duration of the calculation depends essentially on the velocity of the flow solver, and more precisely the convergence of the heat flux.

4.1 Numerical accuracy

A study to estimate the numerical error induced by the flow-grid has been performed, using three grids of different sizes. The number of surface grid points is the same in all three meshes, only the number of prismatic layers has been changed. Indeed, the heat flux at the surface of the vehicle is calculated using the temperature gradient. In Eq. 9, the simplified

heat balance described in Eq. 1 is presented, on the left hand side there is the conductive term and on the right the conductive and the radiative:

$$-\lambda_f \left(\frac{\delta T}{\delta x} \right)_f = -\lambda_s \left(\frac{\delta T}{\delta x} \right)_s + \epsilon \sigma T_w^4 \quad (9)$$

Therefore, maintaining constant the thickness of the prismatic layers, the first spacing and the number of prismatic layers are changed. Thus, the resulting y^+ and the temperature gradient near the wall are better estimated. The three meshes studied have the following characteristics, summarised in Table 1.

	Number of points	Number of prismatic layers
Fine	292906	40
Standard	211092	32
Coarse	176422	24

Table 1: Flow meshes: number of points and prismatic layers.

The accuracy of the meshes is detailed in Table 2. The maximal error is in the stagnation point region, since the other parts of the nose cap the gradients are not so strong and the numerical error is lower. At the stagnation point, an error of 2.67% in the heat flux for the standard grid and in the order of 3.2% for the the coarse grid is obtained. The mean error of the standard grid referred to the fine is between 1% and 1,2%. It turns out all three grids are well passed for the problem here concerned.

	$q[\text{MW/m}^2]$	$\Delta q[\text{MW/m}^2]$	$\epsilon[\%]$	$T[\text{K}]$	$\Delta T[\text{K}]$	$\epsilon[\%]$
Fine	1.816	-	-	2442.35	-	-
Standard	1.767	0.0486	2.67	2439.04	3.31	0.13
Coarse	1.759	0.0562	3.1	2437.1	5.25	0.21

Table 2: Numerical accuracy of the flow meshes.

The numerical error of the thermal model has also been investigated. Using practically structured grids, described in Table 3, the program provides quite accurate solutions also for quite coarse grids, in the order of 2 K regarding to the finest. Although a coarse mesh could be used, a fine mesh is chosen so that the interpolation error is kept minimal. Simulations using the standard flow grid and different thermal meshes show that, the coarser the grid is, the lower the resulting stagnation point temperature. A grid convergence study for a combination of flow/thermal grids indicates a 3,3% error in heat flux and 0,2% error in temperature as a maximum, see Table 6.

	Number of points	Number of surface elements
Fine	17034	614
Standard	7123	351
Coarse	985	152

Table 3: Description of the structural meshes.

In Fig.6 the standard fluid/thermal meshes used for the unsteady simulations are shown, as well as a zoom on the stagnation point regions and on the back part of the nosecap. The thermal mesh is coarse compared to the fluid mesh.

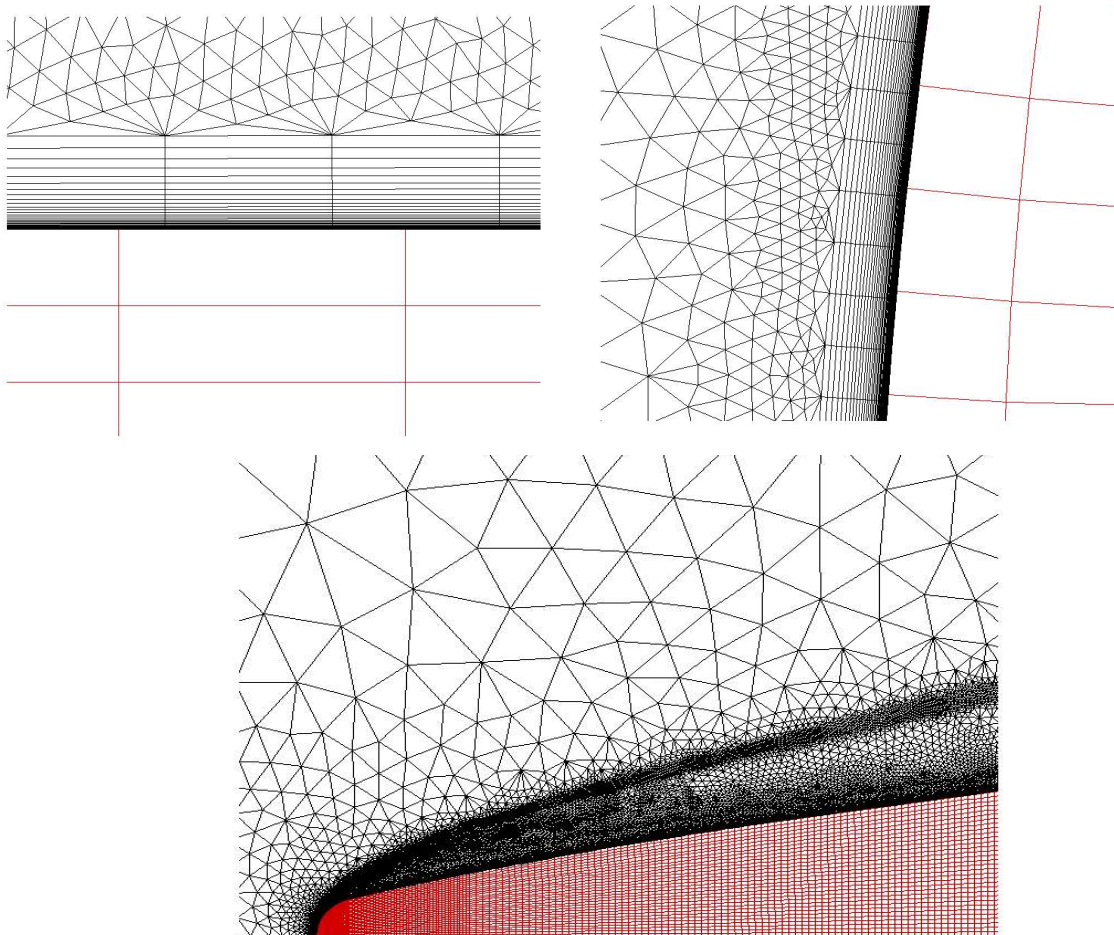


Figure 6: Thermal and Fluid meshes used for the calculation. a) Zoom on the back part of the vehicle. b) Zoom on the stagnation point region. c) Structural and fluid meshes in the nosecap region.

5 RESULTS

At first, a steady state simulation at the first point of the trajectory is performed. Then, an unsteady simulation for the same point is done to verify that the algorithm works by reaching the steady state temperature. Finally, the evolution of the temperature along the trajectory is obtained and compared with the engineering method. The first part of the coupled analysis consists of a steady state simulation for the first point of the trajectory. The structure model corresponds to a projectile made of C/C-SiC. The same algorithm described in Fig. 5 is implemented, but without the time loop and performing a steady state analysis in the thermal solver. The algorithm is initialised with a radiative equilibrium solution for an isolated body and the iterative process repeated until convergence is achieved. To obtain the solution the temperature applied as a BC in the DLR-Tau solver is relaxed in order to improve the convergence of the algorithm: $T_{f_{it}} = wT_{f_{it}} + (1-w)T_{f_{it}}$, where T_f is the temperature applied in the flow solver as BC, and the relaxation factor to 0,35. The results of the algorithm are shown in Table 4.

Iteration	T[K]	ΔT [K]	q[MW/m ²]	Δq [MW/m ²]	Global residual[%]
Radiative Equilibrium	2439.04	-	1.775	-	-
Iteration 1	2377.89	61.15	3.302	1.527	1.57E-002
Iteration 2	2356.99	20.9	3.766	0.466	1.61E-002
Iteration 3	2359.50	2.51	3.685	0.081	4.68E-003
Iteration 4	2356.37	3.13	3.767	0.082	5.01E-003
Iteration 5	2358.74	2.37	3.684	0.083	2.27E-003
Iteration 6	2359.83	1.1	3.700	0.016	1.45E-003
Difference	79.79	-	1.925	-	-

Table 4: Convergence of the solution, steady-state case.

This case is the most restrictive because the temperature variation is quite high. The temperature difference between the flow solution and the one given by the structural solver in the first iteration is 200 K, which is a high value. Therefore, the heat flux obtained in the next iteration is fast two times higher than the radiative equilibrium for an isolated body, and the temperature has to be relaxed. In the solution process, the temperature at the stagnation point oscillates up to 5-6 iterations until it reaches its final value. The chosen criteria is the stagnation point region temperature because the other points of the surface converge within the first or second iterations. The converged solution shows that heat flux at the stagnation point increases almost a factor 2 while the temperature decreases 3,3% (80 K). The difference between both values is due to the extreme conduction of the heat from the stagnation point

region, where the heat flux is relatively high in comparison with the other parts of the vehicle.

In the unsteady approach no relaxation of the temperature is necessary since the variation can be controlled assigning properly the time steps. The oscillation is not so high because the elapsed time does not change the temperature so much as in the steady case. For the trajectory simulations, the minimum number of iterations within a given time interval is 2. Here is presented also the temperature oscillation between iterations for each time step to show the error induced by the algorithm. The unsteady algorithm is robust because of the inner iterations. And, if the obtained heat flux during a time interval is higher than the heat flux of equilibrium of the iteration, the value of the heat flux during the next time interval will be lower than the equilibrium iteration. Thus, if the algorithm does not oscillate, the solution is always kept under these error estimations. Figure 7 presents of the left side the temperature and the heat flux of the steady case. On the right side the results of the unsteady simulation for the first point of the trajectory, as well as the results along the trajectory presented in the next point. The purpose of this simulation is to verify that the unsteady algorithm reproduces the steady state solution achieving the equilibrium temperature and heat flux.

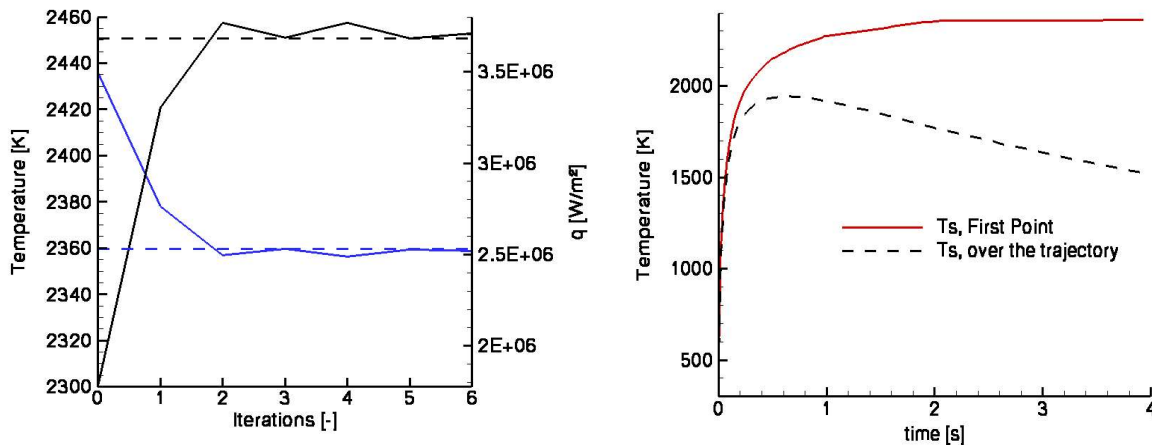


Figure 7: a) Steady coupled solution, temperature and heat flux. b) Unsteady results of the first point of the trajectory.

The steady simulation with the Whipox material presents the same behavior, but due to the lower thermal conductivity, the equilibrium temperature is near the radiative equilibrium one. The results are summarised in Table 5.

	T[K]	ΔT[K]	q[MW/m²]	Δq[MW/m²]
Radiative equilibrium	2478.74	-	1.07	-
Coupled solution	2455.01	23.74	1.32	0.25

Table 5: Convergence of the solution, steady-state case.

Finally, the results of the grid convergence study, described in point 3, are presented in Table 6. The conclusion is that all the considered meshes are adapted to solve the problem.

Fluid/Thermal	Ts[K]	q[MW/m ²]	Δq[MW/m ²]	ΔTs[K]	ε _T [%]	ε _q [%]
Fine/Fine	2355.17	3.62	0.00	0.00	0.00	0.00
Fine/coarse	2352.42	3.11	0.51	2.75	0.12	15.00
Stand./Stand.	2360.00	3.50	0.17	4.60	0.20	3.30

Table 6: Convergence of the solution, steady-state case.

5.1 Temperature evolution along the trajectory

To calculate the temperature along the trajectory three flow meshes are used to fasten the calculation along the trajectory. With the first mesh we calculate the first 4,5 seconds, with the second one from 4,5 to 16,5 seconds, and with the third until the end of the simulation. The y^+ in the stagnation point region is always under 0,1. This procedure guarantees that the boundary layer, as well as the angle of the shock wave are represented by the flow grid.

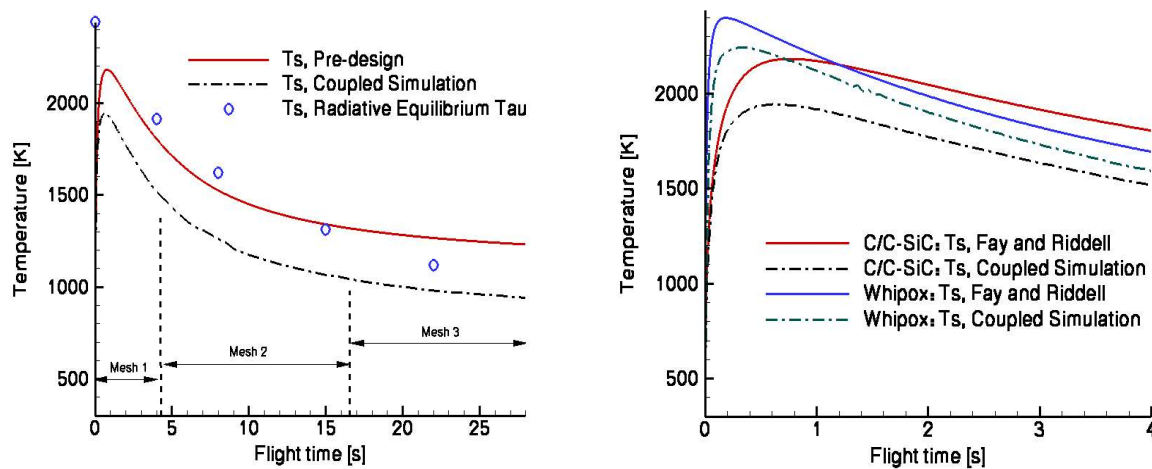


Figure 8: Temperature profiles at the stagnation point over the time. a) Comparison between the coupled method, Fay-Riddell, and the radiation adiabatic solution. b) Temperature evolution during the first 4 seconds of the trajectory for both materials.

Figure 8a shows the evolution of the temperature along the trajectory for the C/C-SiC material. Three methods are compared, the coupled simulation, the radiative equilibrium temperature for an isolated body obtained with DLR-Tau, and the pre-design method. The maximal temperature in the coupled method is reached after 0,76 seconds with a value of 1948K, well under the 2439K of the radiative equilibrium temperature at the first point of the trajectory. In the pre-design method the maximal temperature is also reached after 0.76

seconds with a value of 2181,8 K. The difference between both maximal temperatures is 231K and their evolutions are almost parallel over the time. The temperature of the vehicle tends to the radiative equilibrium one for an isolated body. As the maximal temperature is reached within the first second of the trajectory and then the evolution is parallel to the one obtained with the pre-design tool, only the first four seconds of the trajectory have been calculated for the Whipox material, Fig. 8b. The results are presented on the right hand side of the same figure. The lower conductivity and emissivity of Whipox lead to a higher temperature in the first instants of the trajectory, the temperature reaches a value of 2185 K after 0,3 seconds. The pre-design method reaches 2397 K after 0,2 seconds, the difference is 212 K. The evolution of both algorithms after achieving the maximal temperature is also almost parallel. For both materials the difference between the pre-design and the multidisciplinary solutions is around 200K.

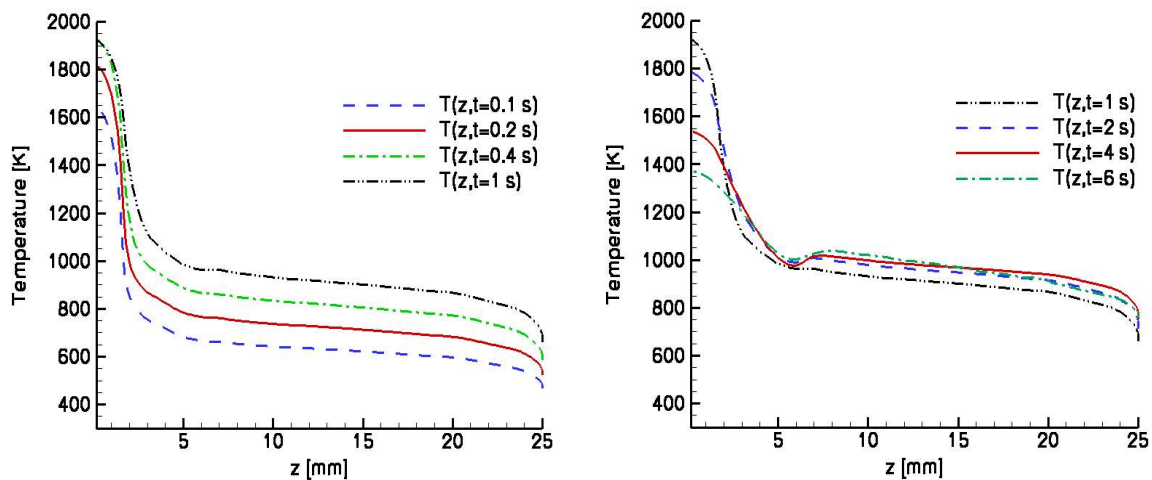


Figure 9: Temperature profiles along the surface of the vehicle as a function of time for the C/C-SiC material.

The temperature profiles along the surface of the projectile for different time sequences are shown in Fig.9. The temperature is presented as a function of z (see coordinate system in Fig. 2b) in order to see better its evolution in the stagnation point region, in the range of 0 to 1,67. During the first second, the temperature overall increases and the profiles are quite parallel because not enough time has passed in order to see the effects of the conduction. Then, the temperature at the stagnation point region reaches its maximum value and the changes between time steps are minimal, while the other regions continue to heat up. Then, the temperature at the stagnation point region decreases while on the other regions continues to increase. It is also remarkable the effect of the bulk-shell, which is situated near $z=6$ mm. In this time interval the effects of the conduction make the temperature raise away from the stagnation point region. This expresses the fact that the dynamic of the temperature is slower in the other regions than in the stagnation point region. Finally, in Fig.10 the temperature field is

presented at two time instants of the trajectory for both materials to its distribution inside the structure.

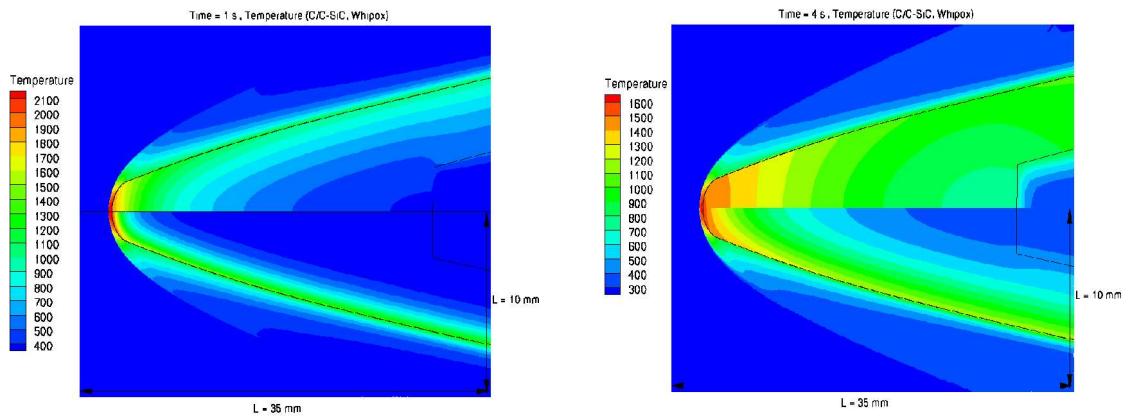


Figure 10: a) Temperature inside and on the flow field, $t = 1$ s. Over: C/C-SiC, under: Whipox. b) Temperature inside and on the flow field, $t = 4$ s. Over: C/C-SiC, under: Whipox.

5.2 Comments on the pre-design method

The evolution of the temperature for both analytical solutions of the heat diffusion equation lead to the same results in the heating phase, as seen in Fig. 11. The high value of the heat flux and also that not enough time has passed, so that the heat can be transported from the surface to the inner regions. This contrasts with the phase after the maximum, in which the length of the slab matters. The lower the thickness of the slab is, the faster cools down the wall.

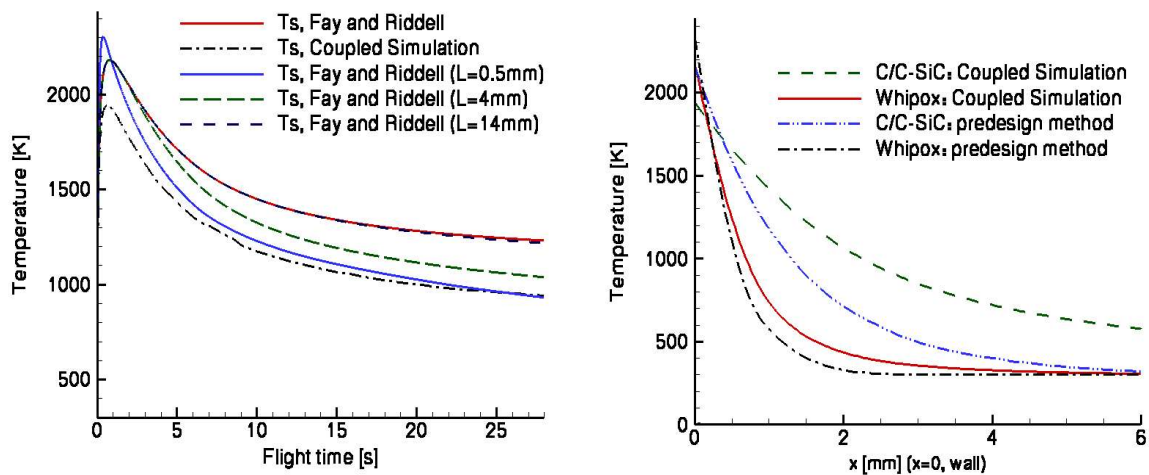


Figure 11: Evolution of the temperature, Fay-Riddell method for different wall lengths compared to the coupled solution.

The differences in the results between both methods are due to the approximations made on the structural model. On one side, the conduction along the surface is not taken into account in a one-dimensional model, this leads to a higher temperature at the stagnation point. The second point in which the solutions differ is the temperature inside the wall. Indeed, if the profiles obtained in a fully coupled solution are compared to the ones obtained using the one-dimensional model. The observed difference, Fig.11, is that the temperatures are higher in the coupled method. Although the temperature at the surface of the vehicle is higher for a pre-design method, the points inside the wall present a lower temperature when we are considering a one-dimensional. This is caused by the neglect of the heat coming from the other parts of the surface to the inner parts of the structure.

6 CONCLUSIONS

This paper has presented the main differences between a fully coupled simulation and a pre-design method. It is a particular case of trajectory, in which the vehicle leaves the electromagnetic accelerator at a hypersonic speed, leading to a very high high flux at the beginning of the trajectory. Therefore, an accurate simulation of the first instants of the flight is needed to estimate the maximum temperature reached by the vehicle. The comparison between the coupled and the pre-design methods for different materials show an offset of 200K (10,25%) due to the simplifications made in the structural model. The results also show, for this type of trajectory, that the maximal temperature reached by the vehicle is high, nevertheless it is maintained only during the first few seconds.

The different material properties and the thermal product characterise the heating of the structure as it is seen in the results for both materials. The thermal product characterises the heating, and the thermal conductivity plays a major role considering the temperature in the inner parts of the structure. The higher this value is, the higher the temperatures are inside the structure. The results show a difference in the order of 500K (25%) between the radiative equilibrium temperature for an isolated body and the coupled simulation. This is due to the heat conduction during the first seconds of the trajectory, and to the thermal characteristics of the material.

The mass of the TPS in such a vehicle represents a high percentage of the total mass. This type of simulation enables a better estimation of the temperatures at the surface and inside the vehicle. Thus, the thicknesses of the outer layer as well as the insulation layer can be better designed. For this trajectory, the differences between the approaches are high, the radiative equilibrium temperature and the maximal obtained with a coupled simulation differ in a 25%. Thus, the calculation of the thicknesses between the approaches are to take into account.

7 ACKNOWLEDGEMENTS

The authors of the paper would like to thank J.M Longo for his help and advice during the realisation of this work.

REFERENCES

- [1] J. Behrens, P. Lehmann, J. Longo, O.Bozic, M. Rapp, and A. Conde Reis, Hypersonic and Electromagnetic Railgun technology as a future alternative for the launch of suborbital payloads, *16th ESA Symposium on Rocket and Balloon Programmes, St. Gallen (CH)*, (2003).
- [2] O. Bozic, J.M. Longo, P. Giese, and J. Behrens, High-end concept based on hypersonic two-stage rocket and electromagnetic railgun to launch micro-satellites into low-earth-orbit, *Fifth European Symposium on Aerothermodynamics for space vehicles, Cologne* (2004).
- [3] H. Hald, Operational limits for reusable space transportation systems due to physical boundaries of C/SiC materials, *Aerspace Science and Technology*, **7**, 551-559 (2003).
- [4] H. Schneider, M. Schmäcker, J. Göring, Kanka B., She S., and Mechnich P, Prouse Alumino Silicate Fiber/Mullite Matrix Composites: Fabrication and Properties, *Ceram. Trans.*, Vol. 115, Westerville, OH: Am. Ceram. Soc. (2000).
- [5] R. D. Quinn, L. Gong, A Method for Calculating Transient Surface Temperature and Surface Heating Rates for High-Speed Aircraft, NASA TP 2000-209034 (2000).
- [6] F. Seiler, U. Werner, G. Patz, Ground Testing Facility for Modeling Real Projectile Flight Heating in Earth Atmosphere, *Journal of Thermophysics and Heat Transfer*, Vol. 16, No.1, 101-108 (2002).
- [7] A. Mack, V. Hannemann, *Validation of the Unstructured DLR-TAU-Code for Hypersonic Flows*, AIAA Paper 2002-3111 (2002).
- [8] John D. Anderson, *Hypersonic and High Temperature Gas Dynamics*, McGraw-Hill Series on Aeronautical and Space Engineering, New York 1989.
- [9] A. Mack, R. Schäfer, Fluid Structure Interaction on a Generic Body-Flap Model in Hypersonic Flow, *Journal of Spacecraft and Rockets*, Vol. 42, No. 5 (2005).
- [10] R. Schäfer, A. Mack, E. Burkard, and A. Gülhan, Fluid-Strcture interaction on a generic model of a reentry vehicle nose cap, *ICTS 5th congress on thermal stresses and related topics*, Blacksburg, Virginia, USA 2003.
- [11] R. Savino, M. De Stefano Fumo, D. Paterna, M. Serpico, Aerothermodynamic study of UHTC-based thermal protection systems, *Aerospace Science and Technology*, **9**, 151-160 (2005).
- [12] F. Infed, F. Olawosky, and M. Ausweter-Kurtz, Stationary Coupling of 3D Hypersonic Nonequilibrium Flows and TPS Structure with Uranus, *Journal of Spacecraft and Rockets*, Vol. 42, 0022-4650 (2005).
- [13] N. Billiard, V. Iliopoulouv, F. Ferrara, R. Denos, Data reduction and thermal product

determination for single and multi layered substrates thin film gauges, *16th Symposium on Measuring Techniques in transonic and supersonic flow in cascades and turbomachines*, Cambridge, United Kingdom (2002).

- [14] H. Julian Allen, A. J. Eggers Jr., A Study of the Motion and Aerodynamic Heating of Ballistic Missiles Entering the Earth's Atmosphere at High Supersonic Speeds, *NACA Technical Report 1381, Forty-Fourth Annual Report of the NACA*, Washington, D.C. (1959).